DRAFT VERSION MAY 11, 2011
Preprint typeset using LaTeX style emulateapj v. 03/07/07

arXiv:1002.1712v3 [astro-ph.CO] 10 May 2011

GROWING MASSIVE BLACK HOLE PAIRS IN MINOR MERGERS OF DISK GALAXIES

SIMONE CALLEGARI[1], STELIOS KAZANTZIDIS[2], LUCIO MAYER[1,3], MONICA COLPI[4],
JILLIAN M. BELLOVARY[5], THOMAS QUINN[6], AND JAMES WADSLEY[7]

Draft version May 11, 2011

ABSTRACT

We perform a suite of high-resolution smoothed particle hydrodynamics simulations to investigate the orbital decay and mass evolution of massive black hole (MBH) pairs down to scales of ~ 30 pc during minor mergers of disk galaxies. Our simulation set includes star formation and accretion onto the MBHs, as well as feedback from both processes. We consider 1:10 merger events starting at $z \sim 3$, with MBH masses in the sensitivity window of the Laser Interferometer Space Antenna, and we follow the coupling between the merger dynamics and the evolution of the MBH mass ratio until the satellite galaxy is tidally disrupted. While the more massive MBH accretes in most cases as if the galaxy were in isolation, the satellite MBH may undergo distinct episodes of enhanced accretion, owing to strong tidal torques acting on its host galaxy and to orbital circularization inside the disk of the primary galaxy. As a consequence, the initial 1:10 mass ratio of the MBHs changes by the time the satellite is disrupted. Depending on the initial fraction of cold gas in the galactic disks and the geometry of the encounter, the mass ratios of the MBH pairs at the time of satellite disruption can stay unchanged or become as large as 1:2. Remarkably, the efficiency of MBH orbital decay correlates with the final mass ratio of the pair itself: MBH pairs that increase significantly their mass ratio are also expected to inspiral more promptly down to nuclear-scale separations. These findings indicate that the mass ratios of MBH pairs in galactic nuclei do not necessarily trace the mass ratios of their merging host galaxies, but are determined by the complex interplay between gas accretion and merger dynamics.

Subject headings: black hole physics — cosmology: theory — galaxies: evolution — hydrodynamics — methods: numerical

1. INTRODUCTION

The ubiquity of massive black holes (MBHs) at the centers of galactic spheroids (Richstone et al. 1998) together with the "bottom–up" nature of galaxy formation in the currently favored ΛCDM cosmology (e.g., White & Rees 1978) suggest that MBH pairs at sub-kpc scales should form in galactic nuclei during the hierarchical assembly of structures (Begelman et al. 1980; see the recent review by Colpi & Dotti 2009). Such pairs may undergo further orbital decay, become Keplerian binaries, and eventually coalesce via the emission of gravitational waves (Haehnelt 1994), which will be one of the main targets of the next generation of gravitational wave detectors such as the Laser Interferometer Space Antenna (LISA) (Vecchio 2004). Moreover, observations indicate that the masses of MBHs correlate with properties of their host spheroids, including the luminosity, mass, and velocity dispersion (e.g., Magorrian & al. 1998; Ferrarese & Merritt 2000; Gebhardt & al. 2000). Such relations suggest the existence of fundamental physical mechanisms that link MBH assembly and galaxy formation, and may connect the properties of galaxy mergers with the resulting MBH binaries.

[1] Institute for Theoretical Physics, University of Zürich, Winterthurerstrasse 190, CH-9057 Zürich, Switzerland; callegar@physik.uzh.ch
[2] Center for Cosmology and Astro-Particle Physics; and Department of Physics; and Department of Astronomy, The Ohio State University, 191 West Woodruff Avenue, Columbus, OH 43210 USA.
[3] Institut für Astronomie, ETH Zürich-Hönggerberg, Wolfgang-Pauli-Strasse 16, CH-8093 Zürich, Switzerland.
[4] Dipartimento di Fisica G. Occhialini, Università di Milano Bicocca, Piazza della Scienza 3. I-20126 Milano, Italy.
[5] Department of Astronomy, University of Michigan, 830 Dennison Bldg., 500 Church Street, Ann Arbor, MI 48109-1042, USA
[6] Department of Astronomy, University of Washington, Box 351580, Seattle, WA 98195, USA.
[7] Department of Physics and Astronomy, McMaster University, 1280 Main Street West, Hamilton, ON L8S 4M1, Canada.

Given all these facts, the study of the dynamics of MBHs during galaxy mergers becomes especially important as a means to connect the cosmological assembly of galaxies with that of MBH pairs and binaries. Many numerical studies have focused on the connection between galaxy mergers and MBH growth, specifically in relation to the MBH final mass, scaling relations and phenomenology of quasars (e.g., Di Matteo et al. 2005; Hopkins et al. 2005; Boylan-Kolchin & Ma 2007; Younger et al. 2008; Johansson et al. 2009). However, much less attention has been devoted to investigating the orbital decay and evolution of both MBHs *during* mergers, particularly in the unequal-mass regime which comprises the vast majority of such events. Kazantzidis et al. (2005) and Callegari et al. (2009) (hereafter C09) showed that the formation of unequal-mass MBH close pairs at sub-kpc scales is sensitive to the details of the gas dynamics during the merger process. In particular, they found that, due to the combination of gas dynamics and star formation, a pair of MBHs can form efficiently in 1:10 minor mergers at scales below 100 pc, provided that galaxies are relatively gas-rich and that the mergers occur at relatively high redshift ($z \sim 3$) when halo densities are higher and dynamical friction timescales correspondingly shorter, according to the Chandrasekhar (1943) standard formulation. However, these papers did not model the accretion onto the MBHs, the evolution of their mass ratio and its dependence on the merger dynamics. Such investigations are important, as the mass ratio of MBH pairs is a fundamental parameter which drives their evolution on nuclear scales (e.g., Dotti et al. 2007; Lodato et al. 2009).

In this paper, we explore in detail for the first time the formation and mass evolution of close MBH pairs down to scales of ~ 30 pc using controlled smoothed particle hydrodynamics (SPH) simulations of minor mergers between disk galax-

ies. The merging systems have a mass ratio of 1 : 10 and our simulation suite includes the effects of star formation and accretion onto the MBHs, as well as feedback from both processes. We model merger events associated with MBH pairs whose gravitational wave emission should be in the sensitivity window of LISA: they have masses $\sim 10^5$ $M_\odot$ around the epoch of a predicted peak of MBH pair formation in mergers happening at $z \sim 3$ (Volonteri et al. 2003; Sesana et al. 2005).

2. NUMERICAL SIMULATIONS

Our reference galaxy model is a $z = 3$ progenitor of a Milky Way-type disk galaxy, with a virial velocity $V_{\rm vir} = 145$ km s^{-1}. Such a progenitor is constructed assuming a constant $V_{\rm vir}$ between redshift 0 and 3 (Li et al. 2007), and rescaling the mass and size of a $z = 0$ model by the ratio $\left[H(z=3)/H_0\right] = 0.224$ of the Hubble constant at $z = 3$ over its present-day value (Mo et al. 1998) for a ΛCDM concordance cosmology ($H_0 = 70$ km s^{-1} Mpc^{-1}, $\Omega_{\rm m} = 0.3$, $\Omega_\Lambda = 0.7$). The model consists of three components: a dark matter halo, a stellar and gaseous disk, and a stellar bulge. The halo is a spherical Navarro et al. (1996) model with a virial mass of $M_{\rm vir} = 2.3 \times 10^{11} M_\odot$, a spin parameter $\lambda = 0.04$ (Vitvitska et al. 2002), and a concentration $c = 3$ consistent with the relations found by Bullock et al. (2001). The halo has been adiabatically contracted to respond to the growth of the disk and bulge (Blumenthal et al. 1986). The baryonic disk follows an exponential profile, with a total mass $M_d = 0.04 M_{\rm vir}$, a radial scale-length $R_d = 1.1$ kpc determined according to Mo et al. (1998), a scale-height of $z_d = 0.1 R_d$, and a mass fraction in gas denoted by $f_{\rm g}$. The bulge is a spherical Hernquist (1990) model with a mass $M_b = 0.008 M_{\rm vir}$, yielding a ratio of bulge-to-total stellar mass $B/T \sim 0.2$ (depending on $f_{\rm g}$), and a scale radius $a_b = 0.2 R_d$. The satellite galaxies are constructed following the same relations between structural parameters and a mass in each component scaled down by $q_{\rm gal} = 0.1$, with a disk scale-length of 300 pc.

The N-body realizations consist of 10^6 particles in the dark matter halo and 2×10^5 stellar particles in each galaxy. In addition, each galaxy is initialized with 10^5 gas particles in the disk, except for one case (see Table 1). We adopted a force resolution of 45 pc for both the dark matter and baryonic particles of the larger galaxy, while for the satellite galaxy we used 20 pc.

A particle representing the MBH was added at the center of each galaxy with a mass according to the updated $M_{\rm BH} - M_{\rm bulge}$ relation of Häring & Rix (2004). Our choice for the galaxy masses in conjunction with the assumption that the MBHs follow the $M_{\rm BH} - M_{\rm bulge}$ relation result in MBH masses of 6×10^4 $M_\odot$ and 6×10^5 $M_\odot$ for the satellite and primary MBH respectively, with an initial MBH mass ratio $q = q_{\rm gal}$. With these choices, we target the typical masses and cosmic epoch of coalescing MBHs that should be detectable by LISA (Volonteri et al. 2003; Sesana et al. 2005).

We choose merger orbital parameters that are common for merging halos in cosmological simulations (Benson 2005). All simulations start with the baricenters of the two galaxies at a distance equal to the sum of their virial radii. Their orbit is initially parabolic, with pericentric distance $R_{\rm p} = 8$ kpc, equal to 20% of the primary galaxy's virial radius, except for one case with a 10 times smaller pericenter. We also vary gas fractions and orbital inclinations. A summary of the simulations here presented can be found in Table 1.[8] All simulations were performed with GASOLINE, a multi-stepping, parallel N-body/SPH code (Wadsley et al. 2004). We include atomic cooling for a primordial mixture of hydrogen and helium, and the star formation algorithm is based on the local Schmidt-Kennicutt law (Katz 1992). Feedback from supernovae is treated using the blast-wave model described in Stinson et al. (2006). Accretion onto the MBHs is also modelled with a sub-grid recipe (e.g., Springel et al. 2005): the accretion rate $\dot{M}_{\rm BH}$ is estimated from the density ρ_g, sound speed c_s and relative velocity V of the gas within a smoothing length from the MBH, via a Bondi-Hoyle-Lyttleton type formula, $\dot{M}_{\rm BH} = 4\pi G^2 M_{\rm BH}^2 \rho_g (V^2 + c_s^2)^{-3/2}$ (Bondi 1952). Of this mass-energy input, a fraction $\epsilon_r = 0.1$ is assumed to be radiated away, while a fraction $(1 - \epsilon_r) = 0.9$ is added to the mass of the MBH from its neighboring gas particles. Lastly, a fraction $\epsilon_{\rm fb} = 0.005$ of the radiated luminosity couples to the surrounding gas as a heating source. This feedback efficiency is tuned so that a number of constraints related to our initial galaxy models can be satisfied (see Section 3.1). In principle, the feedback efficiency depends both on the employed subgrid model for the interstellar medium and the numerical resolution. For all these reasons, our specific choice differs from those used in a number of earlier studies (e.g., Springel et al. 2005). Since the simulations are halted at satellite disruption, the orbital decay of the satellite MBH is determined by the well-resolved drag forces acting on its host galaxy; therefore, we do not include a sub-resolution Bondi drag term, as employed recently by, e.g., Younger et al. (2008). Analogously, we do not employ any other numerical recipe that forces MBH orbital decay, because our aim is to study the growth of MBHs *in relation to the efficiency of close MBH pair formation*. In particular, the black holes were not repositioned at the local minimum of the gravitational potential at each time-step (e.g., Johansson et al. 2009).

TABLE 1
SUMMARY OF MERGER SIMULATIONS

$f_{\rm g}$ primary	$f_{\rm g}$ satellite	θ [b]	notes
30%	30%	0°	reference run
30%	50%	0°	1.7×10^5 SPH particles in the satellite [a]
10%	10%	0°	-
30%	30%	20°	-
30%	30%	45°	-
30%	30%	0°	small pericenter (0.8 kpc)

[a] This number has been chosen in order to have the same ratio of gas particle mass to MBH mass in both primary and satellite galaxies, as happens for all other simulations here discussed.
[b] The orbital plane and satellite disk are inclined by an angle θ with respect to the disk of the primary galaxy.

3. RESULTS

In Section 3.1 our reference simulation is discussed, where the gas fraction in both disks of the primary and satellite galaxy is $f_{\rm g} = 0.3$. Sections 3.2 and 3.3 compare this reference case with other merger simulations of different gas fraction and orbital parameters, respectively, as summarized in Table 1.

3.1. *Reference Simulation: Coplanar Merger with* $f_{\rm g} = 0.3$

[8] We note that only prograde mergers have been considered in this work. In fact, retrograde encounters are characterized by a much slower orbital decay and, particularly in the low mass ratio regime, produce naked "wandering" MBHs as the satellite galaxy is disrupted at distances ~ 10 kpc. From such distances the dynamical friction timescale for producing a MBH pair at ~ 100 pc are longer than a Hubble time.

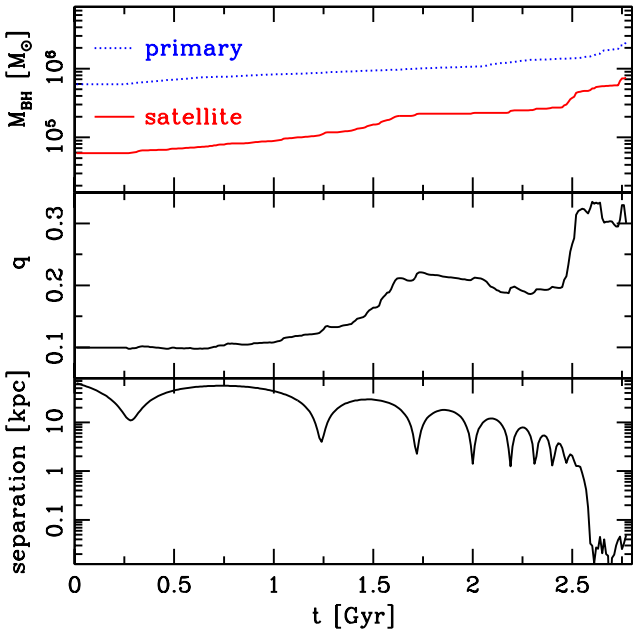

FIG. 1.— Coplanar merger with a disk gas fraction of $f_g = 0.3$ in both galaxies. *Upper panel*: Evolution of the mass of the MBH, M_{BH}, in the primary (dotted line) and satellite galaxy (solid line) as a function of time. *Middle panel*: Evolution of the mass ratio q of the two MBHs as a function of time. *Lower panel*: Orbital decay of the two MBHs as a function of time.

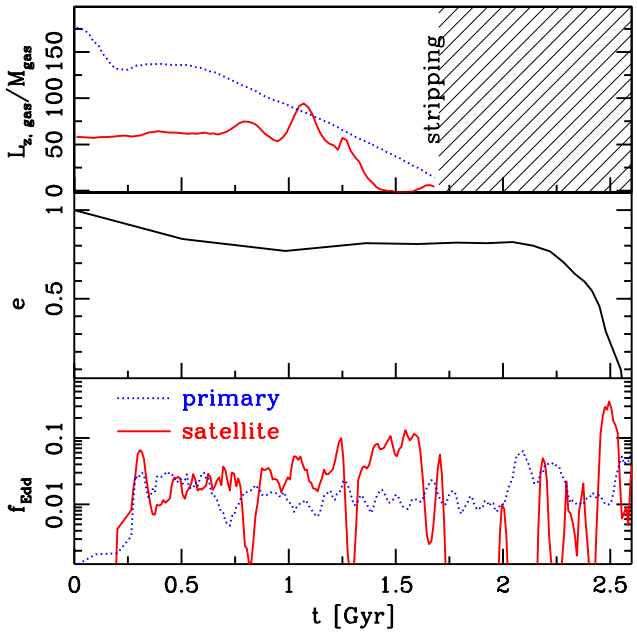

FIG. 2.— Evolution of properties related to the coplanar merger with $f_g = 0.3$ in both galaxies. *Upper panel*: Gas specific angular momentum in the direction of the disk rotation axis in the primary (dotted line) and companion galaxy (solid line) (see text for details). *Middle panel*: Orbital eccentricity of the satellite MBH inside the disk of the primary. *Lower panel*: Eddington ratios, f_{Edd}, of the mass accretion rates onto the primary (dotted line) and secondary MBH (solid line).

In order to assess the effects of the merger on the mass growth of the MBHs, we first performed simulations of the primary and satellite galaxies evolved *in isolation*. For these tests, we chose the $f_g = 0.3$ galaxy models of our reference simulation. In these simulations, the mass ratio of the two MBHs in the isolated galaxies does not deviate significantly or systematically from the initial $q = 0.1$ (the maximum fluctuation around this value is $\sim 10\%$) over a period of more than 2 Gyr. Therefore, we satisfy our working hypothesis that, in equilibrium conditions, the q of the black holes corresponds to the galaxy mass ratio, following from our initial choice of $M_{BH} - M_{bulge}$ and galaxy morphology. In addition, these tests provide a measure of the MBH "quiescent" accretion: mass-doubling timescales of the MBHs evolved in isolation are ~ 2 Gyr, i.e. comparable to the typical duration of one of the mergers presented below. This result indicates that any larger MBH growth or large variation of q during the merger does not stem from secular evolution in the galaxy models or from numerical effects, but rather should be attributed to the galaxy encounter itself.

Figure 1 presents the mass evolution of the two MBHs, the evolution of their mass ratio, and their relative separation as a function of time. By the end of the merger ($t \sim 2.6$ Gyr), owing to dynamical friction, the two MBHs have formed a close pair in the nucleus of the remnant at a separation comparable to the adopted force resolution. This finding confirms our previous results (C09) and suggests that gas accretion onto the MBHs and associated feedback is not critical for pair formation in this case. The primary MBH grows quiescently throughout most of the merger, while the secondary increases its mass tenfold by the time the pair forms. The corresponding increase in the mass ratio of the two MBHs, q, occurs in two distinct episodes, which are elucidated in Figure 2.

The upper panel of Figure 2 shows the evolution of the gas specific angular momentum in the direction of the disk rotation axis, $L_{z,gas}/M_{gas}$, as a function of time for both galaxies. For this calculation, the gas particles that contribute to the baryonic mass within the central 5 softening lengths of each galaxy right before the third pericentric passage ($t = 1.7$ Gyr) were traced back in time. This figure shows that most of the gas in the nuclear region of the satellite at this stage has lost its specific angular momentum on a relatively short timescale. The reason for the angular momentum loss is the strong tidal torques that occur near the second pericentric passage ($t = 1.2$ Gyr) and are induced by the gravitational interaction with the primary galaxy. As a result, a ~ 0.5 Gyr long accretion episode with a corresponding increase of q is observed. As shown in the lower panel of the same Figure, the accretion rate $\dot{M}$ onto the satellite MBH is 10% of the Eddington limit $\dot{M}_{Edd}$ (Eddington 1916) during this phase.

On the other hand, the gas that is funnelled near the center of the primary galaxy has been experiencing a nearly steady loss of specific angular momentum over a very long timescale (Figure 2). This indicates that angular momentum loss in the case of the primary galaxy is not caused by tidal torques arising from the interaction with the satellite, which would occur at pericentric passages and become stronger as the merger progresses. Rather, it is induced by secular evolution (i.e. spiral arms) which redistributes angular momentum throughout the disk. In this context, the effect of initial transient spiral arms is evident during the first ~ 200 Myr. This agrees with the fact that mass growth of the primary MBH is essentially unchanged between the merger and the evolution in isolation.

Around the third pericentric passage, ram pressure exerted by the interstellar medium of the primary galaxy strips all the gas from the satellite down to our force resolution. This is in agreement with analytic estimates based on the study by Marcolini et al. (2003), as discussed also in C09. As a result, the satellite is now devoid of gas (as shown in left panel of

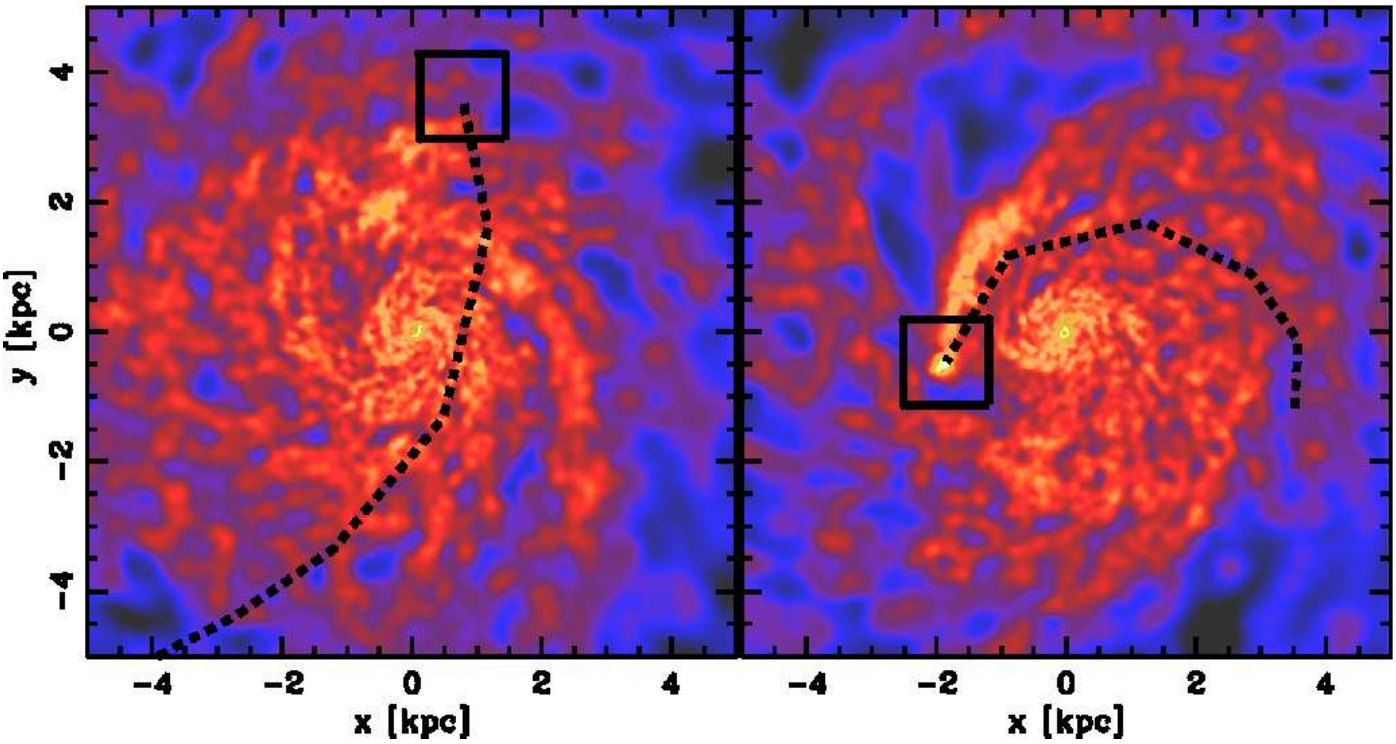

FIG. 3.— Gas density maps at t = 2.33 (left panel) and t = 2.48 Gyr (right panel), which correspond to just before and after the orbit of the secondary MBH circularizes inside the disk of the primary. The time span between these two snapshots corresponds roughly to two orbits of the satellite. The maps show the inner 5 kpc of the primary. Density is projected onto the $x-y$ plane and is color-coded on a logarithmic scale with brighter colors corresponding to regions of higher gas density. The black dashed line marks the trajectory of the satellite MBH and the square indicates the region around it. The satellite does not appear in the left panel, as ram pressure has stripped its entire gas content. On the contrary, the position of the satellite in the right panel is evidently traced by the overdensity and wake excited in the primary disk.

Figure 3), and accretion onto the smaller MBH is suddenly halted. A period of slowly decreasing q follows. In fact, during this phase, the more massive MBH continues to accrete gas from its host, experiencing an increase in its Eddington ratio $f_{\rm Edd} \equiv \dot{M}_{\rm BH}/\dot{M}_{\rm Edd}$ as the satellite galaxy is now orbiting close enough to excite gas inflows in the primary disk ($t > 2$ Gyr).

The mass of the satellite MBH sharply increases again (with an associated second increase in q) at kiloparsec-scale separations. At this stage, the secondary MBH orbits inside the gaseous disk of the primary. The mass increase coincides with a sudden drop in the orbital eccentricity of the satellite MBH, as shown in the middle panel of Figure 2. This drop in eccentricity is caused by dynamical friction acting on the satellite along its prograde coplanar orbit in the high-density region of the primary disk. Such orbit circularization is analogous to that found for MBHs in circumnuclear disks (Dotti et al. 2009). Thus, the satellite MBH and its host stellar cusp are moving with a low relative velocity with respect to the disk of the primary. As a consequence, they are able to collect surrounding gas with low angular momentum in the reference frame of the satellite, creating an overdensity (right panel of Figure 3) from which material is efficiently accreted by the satellite MBH up to a peak $f_{\rm Edd} \sim 0.3$. On the other hand, accretion onto the primary MBH still relies on angular momentum transport by instabilities in the disk. Such instabilities, triggered by the sinking satellite, are stronger than at earlier times, but still not able to sustain high $f_{\rm Edd}$.

Overall, by the time the satellite is disrupted reaching the nuclear region of the merger remnant and the two MBHs form a close pair, the combination of strong tidal torques and orbital circularization acting on the companion galaxy has caused the MBH mass ratio to increase from 1 : 10 to 1 : 3, bringing it into a regime of "major" mass ratio.

3.2. *The Role of Gas Fraction*

Figure 4 compares the evolution of the mass ratio of the MBHs q as a function of time in mergers with different disk gas fractions, $f_{\rm g}$ (see Table1). All of these mergers are on prograde, coplanar orbits. Again, we follow the evolution of the interacting systems up to the time when the orbital decay of the satellite galaxy is completed. This figure shows that the first phase of increase in q, caused by dynamical destabilization of the satellite, happens in all three cases: due to the fact that inclination and orbit are fixed in these mergers, the torques acting on the satellites have the same strength. Interestingly, the highest value of q reached in the first stage traces roughly the amount of gas $\propto f_{\rm g}$ available for MBH fuelling. In all the mergers considered here, ram pressure is effective in removing gas from the satellite galaxy, once the two galaxy disks come into contact. When this happens, accretion onto the secondary MBH is halted.

Figure 4 shows that the initial $f_{\rm g}$ does cause significant differences in the evolution of q also during the second stage of the mergers. Indeed, the second phase of strong accretion onto the satellite MBH is absent in the merger with the smallest gas fraction ($f_{\rm g}$ = 0.1). As discussed earlier, mass growth during this phase becomes efficient only when the secondary MBH moves inside the gas disk of the primary galaxy and its orbit circularizes. Instead, in the case of $f_{\rm g}$ = 0.1 the satellite does not sink below $\sim$ 400 pc before being tidally disrupted, because it has not experienced strong gas inflows steepening its potential well during the first orbits (see C09 for a detailed discussion). At such large distances, the MBH

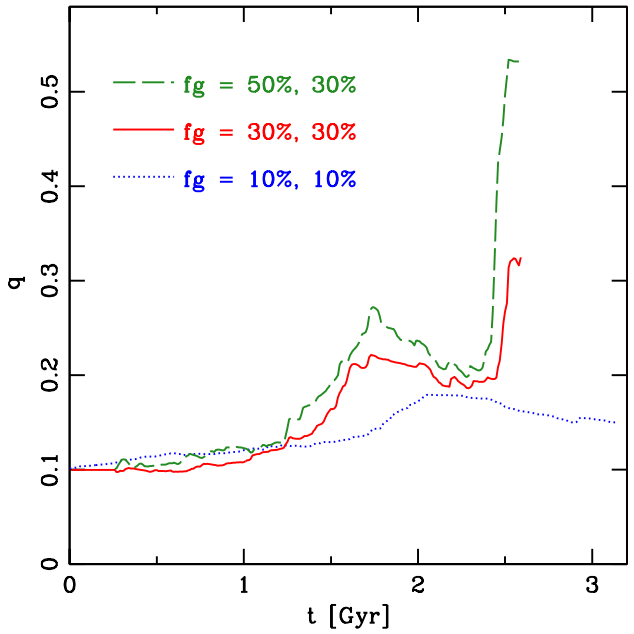

FIG. 4.— Evolution of the mass ratio q of the two MBHs as a function of time in coplanar mergers with different gas fractions f_g. Dotted (blue) and solid (red) lines show results for the mergers with gas fractions $f_g = 0.1$ and $f_g = 0.3$, respectively, in both galaxies. The dashed (green) line corresponds to a merger where the initial gas fractions are $f_g = 0.3$ in the primary and $f_g = 0.5$ in the satellite galaxy.

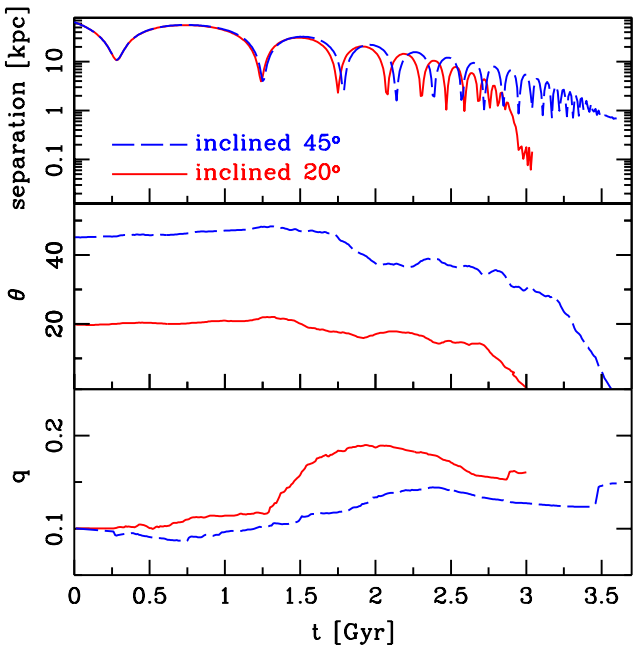

FIG. 5.— The evolution of orbital parameters as a function of time is shown for the inclined runs: the continuous (red) line shows data for the merger with 20° inclination, the dashed (blue) line for the one at 45°. *Upper panel*: MBH separation. As expected, sinking is more effective for more coplanar orbits. *Middle panel*: angle θ between the orbital plane of the two MBHs and the plane of the primary galaxy's disk. Orbit dragging onto the disk plane can be seen in both cases, once the satellite's orbit reaches the disk-dominated region of the primary galaxy. *Lower panel*: Mass ratio of the MBHs.

orbit is still mildly eccentric, and the background density is not high enough to allow for the formation of an overdensity that could trigger the second accretion episode. As a consequence, the MBH mass ratio at the time of satellite disruption is 1:6, close to its initial value, and the naked satellite MBH will still take a few billion years to sink to the center of the remnant via dynamical friction (C09).

We now focus on the merger where the initial gas fraction in the primary and companion galaxies is equal to $f_g = 0.3$ and $f_g = 0.5$, respectively. Figure 4 shows that this case is characterized by a much larger final increase in q compared to our reference case, where the initial gas fraction was equal to $f_g = 0.3$ in both galaxies. Bearing in mind that the only difference between the two initial conditions is the satellite f_g, and that the satellite gas has already been entirely stripped by ram pressure at this late stage, this interesting result can be explained as an effect of the different structure of the surviving satellite core and the different mass growth of its MBH. In fact, a larger initial gas fraction allows the satellite to build a denser stellar core via star formation in response to tidal perturbations during the first two orbits. Consequently, the nuclear region of the satellite is denser and more massive. It is therefore more efficient at collecting gas from the disk of the primary and it is subject to an enhanced sinking. As a result, the orbit of the secondary MBH undergoes circularization in a denser region of the primary disk, and is able to accrete more gas. Moreover, by the time the secondary MBH enters the disk of the primary, it is $\sim 60\%$ more massive compared to the case of $f_g = 0.3$. This difference in mass naturally enhances its accretion rate, which scales as $\propto M_{BH}^2$. At the end of this merger, the satellite MBH has sunk down to the center of the remnant, where a close MBH pair is formed at scales ~ 30 pc, comparable to our force resolution. The mass ratio of the pair at this point is the highest among all our simulations: $q = 0.5$.

3.3. *The Role of Orbital Parameters*

As shown in Sections 3.1 and 3.2, the evolution of the MBH mass ratio depends on processes (especially ram pressure stripping of gas and orbit circularization) that may be sensitive to the initial orbit of the merger itself. In this Section, we discuss results from three simulations addressing the dependence on orbital parameters. In all of them, the gas fraction in the two galaxies was equal to that of the reference case, $f_g = 0.3$.

Upper panel of Figure 5 shows the evolution of the MBH orbital separation in two merger simulations where the orbital plane and satellite disk were inclined with respect to the plane of the primary disk, by 20° in one case, and 45° in the other. Torques acting on the satellite during the early phases of the merger are weaker for higher inclinations (Barnes & Hernquist 1996), and for this reason the increase in mass ratio q during the first three orbits is milder than in the coplanar case with the same gas fraction (Figure 5, lower panel). Moreover, a higher inclination corresponds to a slower orbital decay; in fact, the satellite spends only a small fraction of each orbit in the high density, co-rotating baryonic region of the primary galaxy, where dynamical friction is most efficient. The orbit is eventually dragged down to the plane of the primary disk (Quinn & Goodman 1986) (see middle panel Figure 5). However, since such drag takes a number of orbits to cause significant alignment, the circularization effect – which can only happen when orbiting for most of the time inside the primary disk – is delayed compared to the coplanar case. For this reason, the satellite undergoes a larger number of tidal shocks and is eventually disrupted, precluding a second episode of substantial accretion onto the satellite MBH. For low initial inclination ($\theta = 20°$), the drag is effective enough to bring the MBH down to a separation of

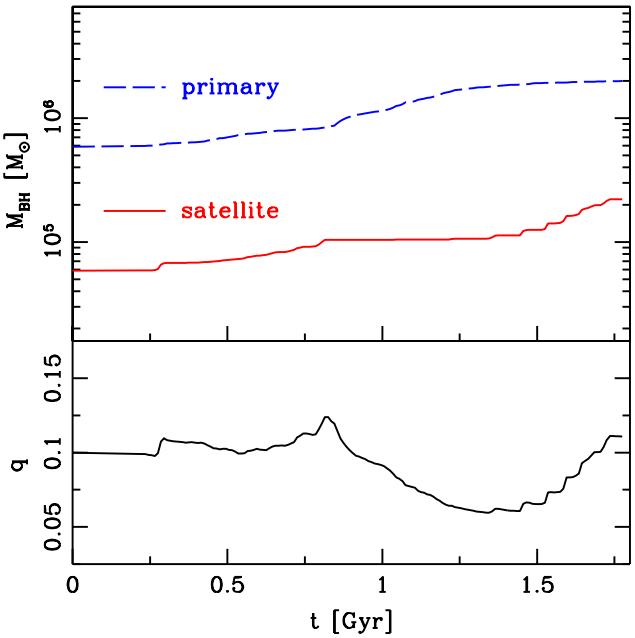

FIG. 6.— MBH evolution in the $f_g = 0.3$ merger with 0° inclination and small pericenter. *Upper panel*: mass accretion of the MBHs. The growth of the satellite MBH stops at second passage ($t = 0.8$ Gyr), earlier than in the other cases, as ram pressure stripping of the satellite gas is more efficient at smaller separations. The primary MBH, on the other hand, starts a period of enhanced accretion after the second orbit, as the perturbations excited onto the primary galaxy are correspondingly stronger. *Lower panel*: evolution of the MBH mass ratio q.

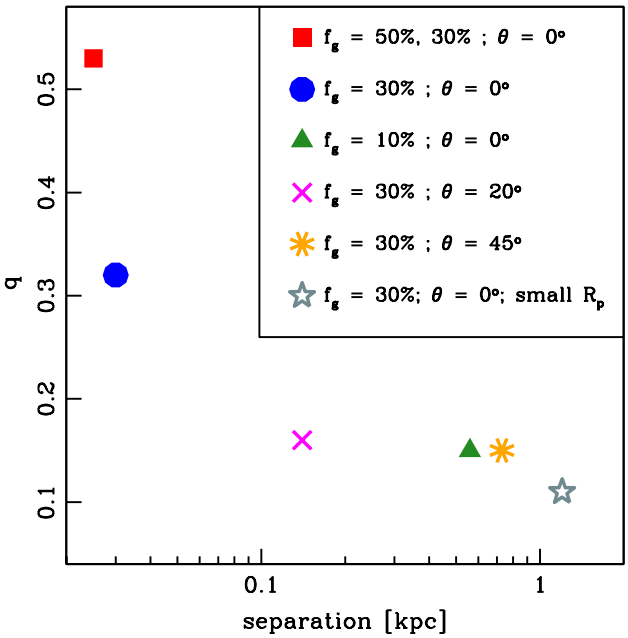

FIG. 7.— The different symbols show the separation of the two MBHs and the corresponding MBH mass ratio q at the time of satellite disruption for all the 1:10 mergers discussed here, labelled according to their initial gas fractions f_g, orbital inclination θ and initial pericenter R_p.

~ 120 pc before the satellite is disrupted. If the inclination is higher ($\theta = 45°$), the satellite is disrupted leaving the MBH at ~ 700 pc distance, where the dynamical friction timescale for sinking of a naked MBH is of a few billion years.

Finally, we turn to the merger starting on a parabolic orbit with very small pericenter (0.8 kpc). The MBH masses and q as a function of time in this case are shown in Figure 6. During the first orbits, the satellite in this merger is subject to stronger tidal torques than in the reference case, but MBH accretion is weaker. This is because the ram pressure acting on the satellite's gas is $P \propto \rho_{ext} V^2$, where ρ_{ext} is the gas density in the primary disk and V is the relative velocity between the satellite and its surroundings. Because of the small distance (corresponding to a high ρ_{ext}) and high V at pericenters, ram pressure stripping is effective since the very first passage: the satellite MBH is starved early and is unable to accrete a substantial amount of mass. For the same reason, MBH growth in the satellite is halted completely already at second pericenter ($t \sim 1.8$ Gyr). On the contrary, the primary MBH experiences enhanced accretion: in fact, the close passages of the satellite excite strong instabilities in the primary disk, funnelling gas towards its nucleus. For this reason, at intermediate times during the merger, the mass ratio drops down to 1 : 20. Analogously to the reference run, a second phase of accretion onto the satellite MBH occurs, in this case bringing q back to its starting value. However, MBH sinking does not proceed any further: as a consequence of the strong tidal shocks experienced by the satellite at pericentric passages, the satellite is disrupted leaving its MBH at a distance of 1 kpc. At these separations, the estimated timescale for orbital sinking of the naked MBH is longer than a Hubble time.

4. DISCUSSION AND CONCLUSIONS

The outcomes of the simulations presented in this Paper are summarized in Figure 7, where the mass ratio q of the MBHs is plotted against their separation, at the time of satellite disruption. As discussed in the previous Sections, the physical processes that facilitate the MBH orbital decay correspond to a stronger accumulation of gaseous mass in the central region of the satellite, compared to the isolated, equilibrium galaxy models. In turn, such gas density enhancement corresponds, in our modelling of black hole accretion, to an increase in the MBH mass ratio. Applying the standard dynamical friction formulation (Chandrasekhar 1943) to a "naked" MBH in our merger remnants, we estimate the timescale for bringing the MBH down to the nuclear region (< 30 pc) to be up to a few billion years for separations up to ~ 1 kpc, and comparable to or longer than a Hubble time for larger separations. Thanks to a combination of stellar-dynamical (e.g., Milosavljević & Merritt 2001) and gas-dynamical (e.g., Gould & Rix 2000; Escala et al. 2005; Dotti et al. 2007) processes, a satellite MBH that sinks down to our current force resolution limit may decay further and form a Keplerian binary together with the primary MBH. Therefore, our results suggest that mergers that may most promptly produce MBH binaries are also those that tend to enhance the MBHs q, with respect to what inferred from the galaxy mass ratio q_{gal}.

Such increase in MBH q happens in two distinct phases, whose occurrence and relative importance depend on the details of the merger process itself. Specifically, in the initial stages of the encounter, the stronger tidal perturbations experienced by the satellite galaxy, compared to those of the primary, cause an enhanced mass growth of its MBH. In addition, in the last stages of the encounter, the orbit of the secondary MBH may circularize inside the disk of the primary. As a result, its ability to accrete gas and grow in mass relative to that of the primary MBH can be further amplified. Such circularization and associated increase in the accretion rate has been previously reported in small-scale simulations of MBH

pairs embedded in a common nuclear disk (Dotti et al. 2009). We note that the amount of gas left around the satellite MBH by ram pressure stripping might be underestimated. In fact, our simulations do not resolve the accretion disk around the MBHs, nor the cold molecular phase in the nuclear region of the satellite; both of these would be less susceptible to ram pressure stripping (e.g., Quilis et al. 2000) and could remain bound to the satellite while the rest of its ISM is lost. In this case, the growth of the secondary MBH may not stop completely and the mass ratios may become even larger.

A cautionary remark concerns the fact that MBH accretion has been modelled assuming the Bondi-Hoyle-Lyttleton sub-grid accretion recipe that is widely used in the literature. However, accretion will most likely occur by means of angular momentum transport in a nuclear disk with an effective α-viscosity (e.g., Lin & Pringle 1987). Other models for gas funnelling and accretion onto central MBHs have been recently proposed to account for the shortcomings of the "standard" approach. Power et al. (2010) propose an accretion scheme for angular momentum-dominated gaseous flows in a stationary gravitational background, introducing a delay in the accretion as a free parameter related to viscous timescales; from their simulations, they find that the Bondi prescription *overestimates* the inflow rate across the MBH influence radius. Hopkins & Quataert (2010) model the transport of angular momentum via disk instabilities arising in galaxy mergers, on scales both larger and smaller than those resolved in this work. They describe the inflow rates down to the MBH sphere of influence with $\dot{M} \sim a M_{\rm g} \Omega$, where $M_{\rm g}$ is the available gaseous mass, Ω the angular speed, and a is related to the amplitude of the instabilities. They find that the Bondi accretion recipe systematically *underestimates* (although with large scatter) the actual inflow rate at sub-pc scales, while better predictions are given by an effective α-disk model. It is therefore unclear whether our accretion recipe introduces a bias in the MBH mass growth, and in which direction. In an attempt to investigate the effect of other sub-grid recipes on our results, we computed *a posteriori* accretion rates in our reference simulation with the recent α-disk sub-resolution model of DeBuhr et al. (2009). We find that such model yields higher $\dot{M}$ compared to the Bondi prescription, in agreement with the findings by Hopkins & Quataert (2010); moreover, the accretion rates onto the two MBHs are enhanced by roughly the same factor. While the absolute values of $\dot{M}$ can depend on the employed numerical prescription, the physical picture concerning the *relative* growth of the two MBHs emerging from our simulations may not be substantially affected by the specific choice of sub-grid modelling. Indeed, our findings reflect clear and well-resolved large scale effects, namely how gravitational torques and orbit circularization can enhance MBH sinking while making a larger gaseous mass relative to $M_{\rm BH}$ available for accretion onto the secondary black hole.

The results presented in this paper are especially relevant in the context of MBH gravitational recoils (Lousto & Zlochower 2009; Tanaka & Haiman 2009). Indeed, if a large fraction of unequal-mass galaxy mergers results in mergers between MBHs with nearly equal masses, then the recoil velocity distribution of the MBH population will be different than expected (e.g., Volonteri et al. 2010). However, the actual recoil velocity distribution will also depend on the magnitude and relative orientation of the spins of the MBHs at the final stage of the merger, which is likely driven by gas dynamics at scales well below those resolved in our simulations (Perego et al. 2009; Dotti et al. 2010).

Our findings, together with those of C09 and of Kazantzidis et al. (2005), confirm the fundamental role of tidal stripping and gas-dynamical effect in deciding the formation and properties of close MBH pairs in unequal-mass galaxy mergers. Moreover, our results suggest that the efficiency of MBH pair formation may correlate with the final mass ratio of the pair itself, so that MBH pairs with larger mass ratios tend to be produced more effectively and promptly. Gravitational wave detectors, such as LISA, will enable the use of gravitational wave signals from MBH coalescences as a new, independent probe of cosmic structure formation. Indeed, gravitational wave-forms can allow the determination of mass, spin, and orbital parameters of the merging MBHs (Vecchio 2004). In principle, this information could be used to infer the masses of the merging host galaxies. However, our results show that this connection cannot be made by simply applying the observed scaling relations between the masses of MBHs and the properties of their host galaxies, even if these scalings are applicable to galaxies throughout cosmic history. The findings presented here suggest that the mapping between galaxy and MBH mergers depends on various factors, such as the gas content of the merging galaxies and the encounter geometry, and as such might need to be approached in a probabilistic way. Such investigations would require a combination of a series of merger experiments that explore a larger parameter space with semi-analytical models of the co-evolution between galaxies and MBHs.

The authors are grateful to Jackson DeBuhr, Massimo Dotti, Marta Volonteri, and David Weinberg for stimulating discussions, and to the anonymous referee for comments that greatly improved this Paper. SC, SK, and LM acknowledge the Kavli Institute for Theoretical Physics at the University of California at Santa Barbara for hosting the workshop "Building the Milky Way" during the initial stages of this work. SC is also grateful to the Center for Cosmology and Astro-Particle Physics (CCAPP) at The Ohio State University for hospitality while completing this work. This research is supported by the Swiss National Science Foundation, by CCAPP, and by an allocation of computing time from the Ohio Supercomputer Center (OSC). Simulations were performed on the IBM Opteron Cluster "Glenn" at OSC and on the zBox3 at the University of Zürich. This research made use of the NASA Astrophysics Data System.

REFERENCES

Barnes, J. E. & Hernquist, L. 1996, ApJ, 471, 115
Begelman, M. C., Blandford, R. D., & Rees, M. J. 1980, Nature, 287, 307
Benson, A. J. 2005, MNRAS, 358, 551
Blumenthal, G. R., Faber, S. M., Flores, R., & Primack, J. R. 1986, ApJ, 301, 27
Bondi, H. 1952, MNRAS, 112, 195
Boylan-Kolchin, M. & Ma, C.-P. 2007, MNRAS, 374, 1227
Bullock, J. S., Kolatt, T. S., Sigad, Y., Somerville, R. S., Kravtsov, A. V., Klypin, A. A., Primack, J. R., & Dekel, A. 2001, MNRAS, 321, 559
Callegari, S., Mayer, L., Kazantzidis, S., Colpi, M., Governato, F., Quinn, T., & Wadsley, J. 2009, ApJ, 696, L89
Chandrasekhar, S. 1943, ApJ, 97, 255
Colpi, M. & Dotti, M. 2009, ArXiv e-prints
DeBuhr, J., Quataert, E., Ma, C., & Hopkins, P. 2009, ArXiv e-prints
Di Matteo, T., Springel, V., & Hernquist, L. 2005, Nature, 433, 604
Dotti, M., Colpi, M., Haardt, F., & Mayer, L. 2007, MNRAS, 379, 956
Dotti, M., Ruszkowski, M., Paredi, L., Colpi, M., Volonteri, M., & Haardt, F. 2009, MNRAS, 396, 1640
Dotti, M., Volonteri, M., Perego, A., Colpi, M., Ruszkowski, M., & Haardt, F. 2010, MNRAS, 402, 682
Eddington, A. S. 1916, MNRAS, 77, 16
Escala, A., Larson, R. B., Coppi, P. S., & Mardones, D. 2005, ApJ, 630, 152
Ferrarese, L. & Merritt, D. 2000, ApJ, 539, L9
Gebhardt, K. & al. 2000, ApJ, 539, L13
Gould, A. & Rix, H. 2000, ApJ, 532, L29
Haehnelt, M. G. 1994, MNRAS, 269, 199
Häring, N. & Rix, H.-W. 2004, ApJ, 604, L89
Hernquist, L. 1990, ApJ, 356, 359
Hopkins, P. F., Hernquist, L., Cox, T. J., Di Matteo, T., Martini, P., Robertson, B., & Springel, V. 2005, ApJ, 630, 705
Hopkins, P. F. & Quataert, E. 2010, ArXiv e-prints
Johansson, P. H., Naab, T., & Burkert, A. 2009, ApJ, 690, 802
Katz, N. 1992, ApJ, 391, 502
Kazantzidis, S., Mayer, L., Colpi, M., Madau, P., Debattista, V. P., Wadsley, J., Stadel, J., Quinn, T., & Moore, B. 2005, ApJ, 623, L67
Li, Y., Mo, H. J., van den Bosch, F. C., & Lin, W. P. 2007, MNRAS, 379, 689
Lin, D. N. C. & Pringle, J. E. 1987, MNRAS, 225, 607
Lodato, G., Nayakshin, S., King, A. R., & Pringle, J. E. 2009, MNRAS, 398, 1392
Lousto, C. O. & Zlochower, Y. 2009, Phys. Rev. D, 79, 064018
Magorrian, J. & al. 1998, AJ, 115, 2285
Marcolini, A., Brighenti, F., & D'Ercole, A. 2003, MNRAS, 345, 1329
Milosavljević, M. & Merritt, D. 2001, ApJ, 563, 34
Mo, H. J., Mao, S., & White, S. D. M. 1998, MNRAS, 295, 319
Navarro, J. F., Frenk, C. S., & White, S. D. M. 1996, ApJ, 462, 563
Perego, A., Dotti, M., Colpi, M., & Volonteri, M. 2009, MNRAS, 399, 2249
Power, C., Nayakshin, S., & King, A. 2010, MNRAS, 412, 269
Quilis, V., Moore, B., & Bower, R. 2000, Science, 288, 1617
Quinn, P. J. & Goodman, J. 1986, ApJ, 309, 472
Richstone, D., Ajhar, E. A., Bender, R., Bower, G., Dressler, A., Faber, S. M., Filippenko, A. V., Gebhardt, K., Green, R., Ho, L. C., Kormendy, J., Lauer, T. R., Magorrian, J., & Tremaine, S. 1998, Nature, 395, A14+
Sesana, A., Haardt, F., Madau, P., & Volonteri, M. 2005, ApJ, 623, 23
Springel, V., Di Matteo, T., & Hernquist, L. 2005, MNRAS, 361, 776
Stinson, G., Seth, A., Katz, N., Wadsley, J., Governato, F., & Quinn, T. 2006, MNRAS, 373, 1074
Tanaka, T. & Haiman, Z. 2009, ApJ, 696, 1798
Vecchio, A. 2004, Phys. Rev. D, 70, 042001
Vitvitska, M., Klypin, A. A., Kravtsov, A. V., Wechsler, R. H., Primack, J. R., & Bullock, J. S. 2002, ApJ, 581, 799
Volonteri, M., Gultekin, K., & Dotti, M. 2010, MNRAS, 404, 2143
Volonteri, M., Haardt, F., & Madau, P. 2003, ApJ, 582, 559
Wadsley, J. W., Stadel, J., & Quinn, T. 2004, New Astronomy, 9, 137
White, S. D. M. & Rees, M. J. 1978, MNRAS, 183, 341
Younger, J. D., Hopkins, P. F., Cox, T. J., & Hernquist, L. 2008, ApJ, 686, 815